Wave spectra of two-dimensional dusty plasma solids and liquids

Lu-Jing Hou,[1,*] Z. L. Mišković,[2] Alexander Piel,[1] and Michael S. Murillo[3]
[1]*IEAP, Christian-Albrechts Universität, D-24098 Kiel, Germany*
[2]*Department of Applied Mathematics, University of Waterloo, Waterloo, Ontario, Canada N2L 3G1*
[3]*Physics Division, Los Alamos National Laboratory, Los Alamos, New Mexico 87545, USA*
(Received 2 February 2009; published 30 April 2009)

Brownian dynamics simulations were carried out to study wave spectra of two-dimensional dusty plasma liquids and solids for a wide range of wavelengths. The existence of a longitudinal dust-thermal mode was confirmed in simulations, and a cutoff wave number in the transverse mode was measured. Dispersion relations, resulting from simulations, were compared with those from analytical theories, such as the random-phase approximation (RPA), the quasilocalized charged approximation (QLCA), and the harmonic approximation (HA). An overall good agreement between the QLCA and simulations was found for wide ranges of states and wavelengths after taking into account the direct thermal effect in the QLCA, while for the RPA and HA, good agreement with simulations was found in the high and low-temperature limits, respectively.

DOI: 10.1103/PhysRevE.79.046412 PACS number(s): 52.25.Fi, 52.27.Gr, 52.27.Lw

I. INTRODUCTION

A laboratory-generated dusty plasma is a suspension of micron-sized particles immersed in a usual plasma with ions, electrons, and neutral-gas molecules [1–3]. Dust particles acquire a few thousand of electron charges by absorbing the surrounding electrons and ions, and they consequently interact with each other via a dynamically screened Coulomb potential [4], while undergoing Brownian motions due to frequent collisions, mainly with the neutral-gas molecules. When the interaction potential energy between charged dust particles significantly exceeds their kinetic energy, they become strongly coupled and, consequently, they can form ordered structures characteristic of a liquid or solid state. Such structures are commonly referred to as strongly coupled dusty plasmas (SCDPs).

Two-dimensional (2D) SCDPs have become particularly favored in recent laboratory experiments and simulations. One of the reasons is that for a 2D dust layer levitating in a plasma sheath, possible complications arising from the ion flow perpendicular to this layer and the accompanying ion wake effect in the downstream direction (see, e.g., [4] and the references therein) are expected to have little or no influence on the interactions between dust particles within the layer. In that context, it was shown both experimentally [5] and theoretically [6] that the interparticle interaction is well approximated by a Yukawa-type potential, which greatly facilitates both the analytical theory and computer simulation.

Of particular interest in 2D dusty plasmas are their collective and dynamical properties, such as longitudinal and transverse wave modes, which have been studied extensively over the past decade in experiments [7–12], theories [13–19], and numerical simulations [18,20,21]. On the experimental side, externally excited (longitudinal) dust lattice waves (DLWs) were first observed by Homann *et al.* [7,8], who found their dispersion relation to be in good agreement with the theoretical prediction of Melandsø [14]. Next, thermally excited phonon spectrum in a 2D plasma crystal was observed in an experiment by Nunomura *et al.* [9], who demonstrated a good agreement of this spectrum with theory [13,15,16] for both the longitudinal and transverse modes in the entire first Brillouin zone. That experiment was later extended by Zhdanov *et al.* [10], who studied the polarization of wave modes in a 2D plasma crystal, and by Nunomura *et al.* [11], who studied the wave spectra in both liquid and solid states for a wide range of wavelengths. More recently, Nosenko *et al.* [12] measured experimentally a critical cutoff wave number for shear waves in 2D dusty plasma liquids.

On the theoretical side, besides the above mentioned DLW theories of Peeters and Wu [13], Melandsø [14], Dubin [15], and Wang *et al.* [16], as well as the standard dust-acoustic wave (DAW) theory [22,23] along with its 2D derivatives [24,25], there have been many other studies of SCDPs. For example, a semianalytic approximation was used to study wave propagation in 2D SCDPs [15,25]. The quasilocalized charge approximation (QLCA) [26] was used to study collective modes and dynamics of both three-dimensional (3D) [27,28] and 2D [18] dusty plasma liquids. Furthermore, a generalized hydrodynamic (GH) model was adopted by Kaw and Sen [29] to study wave dispersion in 3D dusty plasma liquids, while Murillo and co-workers studied collective modes by using both kinetic [30] and the GH [31,32] methods. The latter method was used, in particular, to study critical wave numbers for transverse modes in a 3D dusty plasma in liquid phase [31].

On the other hand, computer simulations [18,20,21,33,34], as an essential supplement to real experiments, have played important roles in validating various analytical theories and in explaining experimental observations. Both molecular dynamics (MD) and the particle-in-cell (PIC) simulations were carried out by Winske *et al.* [33] to study longitudinal wave dispersion in one-dimensional systems. Results were compared with the DAW mode and with the 3D QLCA [27] including the strong-coupling effects, and an agreement with the QLCA was found only at very long wavelengths due to the small system size. Later on, Ohta and Hamaguchi [34] studied both the longitudinal and transverse dispersion relations in 3D dusty plasma liquids, and their

*ljhouwang@gmail.com

results were compared with both the QLCA [27,28] and the GH model [29,31]. It was found that for the longitudinal mode, both theories were in close agreement with simulations in the entire first Brillouin zone, whereas, for the transverse mode, good agreement with simulations was found for both theories, except in the very long-wavelength region, where the GH model successfully predicts a cutoff but the QLCA does not. This deficiency of the QLCA can be rectified by introducing a phenomenological damping which accounts for the diffusional and other damping effects, as was shown more recently in the work by Kalman *et al.* [18], where the QLCA was extended to study 2D dusty plasma liquids, and the results were critically compared with MD simulations. Good agreement with simulations was found for both the longitudinal and transverse modes, mostly in the first Brillouin zone. (Please see Ref. [35] for a nice review of recent development about collective dynamics in 2D and 3D Yukawa liquids.)

However, it should be noted that, first, most of the above simulations [18,20,21,33–35] considered dusty plasmas in the liquid state, and the obtained dispersion relations were limited to the first Brillouin zone. To the best of our knowledge, there are no simulations verifying the above mentioned analytical theories for a wider range of wavelengths, as well as for dusty plasmas in a nonideal gaseous, or in solid states. Second, no simulations have been conducted to examine a transition from the random-phase-approximation (RPA)-based DAW to the harmonic-approximation (HA)-based DLW theories when dusty plasma goes from a high-temperature liquid (or a nonideal gaseous) state to a low-temperature crystalline state. Third, an analytical theory based on the RPA [23] predicted a so-called dust-thermal wave (DTW) due to the direct thermal effect of dust particles, and its existence was verified in a subsequent experiment [11]. However, the original theory [23] applies to weakly coupled systems only, and it would be interesting to study, both analytically and via computer simulation, how the DTW behaves in strongly coupled systems.

To fulfill these goals, we perform here computer simulations and study the resulting wave spectra of 2D dusty plasmas for a wide range of wavelengths and system states. Results are compared with the available analytical theories for the 2D geometry, such as, RPA, QLCA, and HA. In addition, two extensions of the standard QLCA are discussed, one including the direct thermal effect, and the other implementing a critical wave cutoff in the transverse mode, based on the method of Kalman *et al.* [18,35]. The role of damping effects on collective modes is also investigated in the simulation. The remaining part of the paper is organized as follows. Details of our simulations are presented in Sec. II, which is followed by a presentation and discussion of the results in Sec. III, including brief derivations and reviews of various analytical theories. Concluding remarks are given in Sec. IV.

II. SIMULATION

A. Algorithm

Our simulation is based on the Brownian dynamics (BD) method [36–38], which may be regarded as a generalization of the standard MD method. Namely, while the MD simulation is based on Newton's equations of motion, the BD method is based on their generalization in the form of Langevin equation (and its integral), viz.,

$$\frac{d}{dt}\mathbf{r} = \mathbf{v},$$

$$\frac{d}{dt}\mathbf{v} = -\nu\mathbf{v} + \frac{1}{m}\mathbf{F} + \mathbf{A}(t), \tag{1}$$

where, as usual, m, $\mathbf{v}$, and $\mathbf{r}$ are, respectively, the mass, velocity, and position of a Brownian particle, while $\mathbf{F}$ is a systematic (deterministic) force coming from the interparticle interactions within the system and, possibly, from external force fields. What is different from Newton's equations is the appearance of the dynamic friction, $-\nu\mathbf{v}$, and the Brownian acceleration, $\mathbf{A}(t)$, which represent two complementing effects of a single subscale phenomenon: numerous frequent collisions of the Brownian particle with the molecules in the medium. While the former represents the average effect of these collisions, the latter represents fluctuations due to discreteness of the collisions, and is generally assumed to be well represented by a delta-correlated Gaussian white noise. They are both related to the medium temperature through a fluctuation-dissipation theorem.

The Langevin equations [Eq. (1)] may be numerically integrated in a manner similar to the integration of Newton's equations in the MD method, and such a technique is generally called Brownian dynamics. (Note that several different names are used in literature to designate methods for numerical integration of Langevin equation, for example, Brownian dynamics, Langevin dynamics, or Langevin molecular dynamics, depending on the background, area, or preferences of different researchers. Those names may refer to the same technique that we discuss here, or they may involve subtle differences in derivations of the simulation formulas, and/or in implementations of simulation. We follow here definitions given by Allen and Tildesley [36].)

We employ here the fifth-order Gear-like predictor-corrector algorithm [37,38] for BD simulation, which was used successfully in simulating shock wave propagation [39–42], heat conduction [43], and diffusion processes in SCDPs [44]. When compared with several other popular methods for BD simulation, such as Euler-like, Beeman-like, and Verlet-like methods [36], the present method can cover a wider range of friction coefficients ν, and is particularly reliable in the low-damping regime while exhibiting higher-order accuracy, good stability, and negligible drift on long time scales. Therefore, the present algorithm appears to be especially suitable to simulate dusty plasmas, which are often slightly damped.

B. Calculation of wave spectra

Typically, $N=4000$ dust particles are simulated in a square with periodic boundary conditions. As mentioned in Sec. I, particles are assumed to interact with each other via pairwise Yukawa potential of the form $\phi(r)=(e^2Z_d^2/r)\exp(-r/\lambda_D)$,

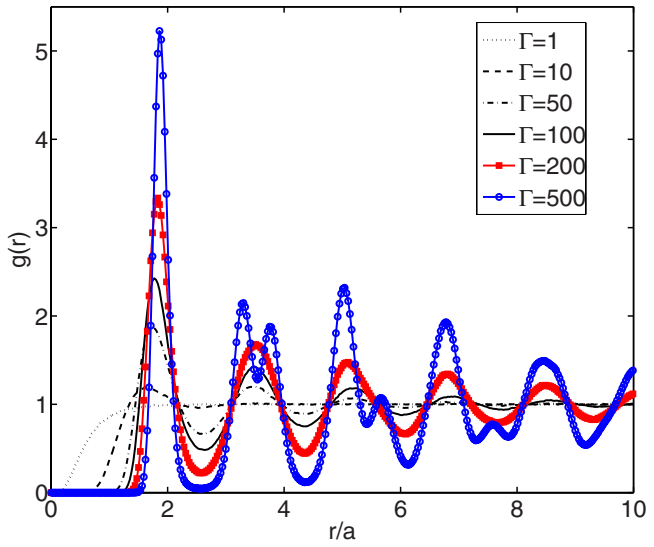

FIG. 1. (Color online) Radial distribution function $g(r)$ for $\kappa=1$ and different Γ.

where e is the elementary charge, Z_d is the average number of charges on each dust particle, r is the interparticle distance, and λ_D is the Debye screening length. Such a system can be fully characterized by three parameters [45]: the Coulomb coupling parameter, $\Gamma=(eZ_d)^2/(aT)$, the screening parameter, $\kappa=a/\lambda_D$, and the damping rate, ν/ω_{pd}, due to the neutral gas, where T is the system temperature (in energy units), $a=(\pi\sigma_{d0})^{-1/2}$ the Wigner-Seitz radius, and σ_{d0} the equilibrium dust number density. The dust plasma frequency is defined by $\omega_{pd}=[2(eZ_d)^2/(ma^3)]^{1/2}$, where m is the dust particle mass. We shall use $\kappa=1$ throughout our simulation and in subsequent discussions because $\kappa\sim 1$ is the most typical value found in experiments [9–12] and, moreover, no substantial effects of varying κ are expected in the features to be discussed in the following.

Initially, dust particles are randomly placed in the square. The system comes to an equilibrium after a period which is proportional to $1/\nu$, and is usually about $10/\nu$. The time step used in simulations is $\delta t=0.02\omega_{pd}^{-1}$ for $\Gamma\geq 10$ and $\delta t=0.01\omega_{pd}^{-1}$ for $\Gamma<10$. After the system reaches an equilibrium, radial distribution function $g(r)$ and wave spectra are calculated. Note that the radial distribution function, $g(r)$, is related to the conditional probability density that if one particle is located at the coordinate origin, another particle will be found in the interval of radial distances $(r,r+dr)$. Figure 1 shows examples of $g(r)$ for $\kappa=1$, with different Γ values. These results will be used as an input below in evaluating the QLCA dispersion relations.

The longitudinal, $\mathcal{L}(\mathbf{k},\omega)$, and transverse, $\mathcal{T}(\mathbf{k},\omega)$, wave spectra are determined by means of the current-current correlation functions in the longitudinal and transverse directions, respectively. We follow Ref. [46], in which the current density of the system is defined by

$$\mathbf{j}(\mathbf{r},t)=\frac{1}{\sqrt{N}}\sum_{i=1}^{N}\mathbf{v}_i(t)\,\delta[\mathbf{r}-\mathbf{r}_i(t)], \tag{2}$$

with the Fourier transform of its Cartesian component α given by

$$j_\alpha(\mathbf{k},t)=\frac{1}{\sqrt{N}}\sum_{i=1}^{N}v_{i\alpha}(t)e^{i\mathbf{k}\cdot\mathbf{r}_i(t)}, \tag{3}$$

where $\mathbf{r}_i(t)$ and $\mathbf{v}_i(t)$ are, respectively, position and velocity of the ith particle at time t, with α being x or y. Assuming that waves propagate along the x direction, i.e., $\mathbf{k}=(k,0)$, one defines

$$J_L(\mathbf{k},t)=\langle j_x^*(\mathbf{k},t)j_x(\mathbf{k},0)\rangle,$$

$$J_T(\mathbf{k},t)=\langle j_y^*(\mathbf{k},t)j_y(\mathbf{k},0)\rangle,$$

to be, respectively, the longitudinal and transverse current autocorrelations. Here, the asterisk designates complex conjugation, while the angular brackets indicate an ensemble average. The longitudinal and transverse wave spectra are then obtained from the Fourier transforms of the corresponding current autocorrelations [46],

$$\mathcal{L}(\mathbf{k},\omega)=\int_{-\infty}^{+\infty}dt e^{i\omega t}J_L(\mathbf{k},t),$$

$$\mathcal{T}(\mathbf{k},\omega)=\int_{-\infty}^{+\infty}dt e^{i\omega t}J_T(\mathbf{k},t). \tag{4}$$

In the simulation, Eqs. (4) are evaluated by using discrete Fourier transform in a period of $1310\omega_{pd}^{-1}$.

III. RESULTS AND DISCUSSIONS

In this section, we present our main simulation results for wave spectra, together with analytical results for dispersion relations for DAW [25], DTW [23], and those obtained by using QLCA [18] and HA [15]. The relevant theoretical derivations are briefly reviewed for the sake of completeness.

A. DAW

Let us begin with a weakly coupled state. We use here a fluid description for a monolayer of dust particles levitating in a background plasma, without considering details of their mutual interactions. Assuming that a cold 2D dust fluid occupies the plane $z=0$ in a Cartesian coordinate system with $\mathbf{R}=(x,y,z)$, we let $\sigma_d(\mathbf{r},t)$ and $\mathbf{u}_d(\mathbf{r},t)$ be, respectively, the number density per unit area and the velocity field (having the x and y components only) of the dust fluid at position $\mathbf{r}=(x,y)$ and at time t. The continuity equation and the momentum equation for the fluid are, respectively [25],

$$\frac{\partial\sigma_d(\mathbf{r},t)}{\partial t}+\nabla_\parallel\cdot[\sigma_d(\mathbf{r},t)\mathbf{u}_d(\mathbf{r},t)]=0, \tag{5}$$

$$\frac{\partial\mathbf{u}_d(\mathbf{r},t)}{\partial t}+\mathbf{u}_d(\mathbf{r},t)\cdot\nabla_\parallel\mathbf{u}_d(\mathbf{r},t)=\frac{eZ_d}{m}\nabla_\parallel\Phi(\mathbf{R},t)|_{z=0}-\nu\mathbf{u}_d(\mathbf{r},t), \tag{6}$$

where ν is the Epstein drag coefficient. Note that the spatial differentiation in Eqs. (5) and (6) includes tangential directions only, viz., $\nabla_\parallel=\hat{\mathbf{x}}\frac{\partial}{\partial x}+\hat{\mathbf{y}}\frac{\partial}{\partial y}$. The first term in the right-hand

side of Eq. (6) indicates that although the total electrostatic potential $\Phi(\mathbf{R},t)$ depends on all three spatial coordinates $\mathbf{R} \equiv (\mathbf{r},z)$, only the x and y components of the electrostatic force, evaluated in the plane $z=0$, affect the motion of the dust fluid. The full spatial dependence of the electrostatic potential Φ is determined from the Poisson equation in 3D,

$$\nabla^2\Phi(\mathbf{R},t) = -4\pi e[n_i(\mathbf{R},t) - n_e(\mathbf{R},t) - Z_d\sigma_d(\mathbf{r},t)\delta(z)], \tag{7}$$

where $\nabla = \nabla_\parallel + \hat{\mathbf{z}}\frac{\partial}{\partial z}$. The electron and ion volume densities are given by the Boltzmann relations, $n_e = n_0 \exp(e\Phi/T_e)$ and $n_i = n_0 \exp(-e\Phi/T_i)$, respectively, owing to the fact that the dynamics of massive dust particles is so slow that both electrons and ions are considered to have enough time to reach their respective local equilibria, with n_0 being the equilibrium plasma density and $T_{i(e)}$ the ion (electron) temperature (in energy units). In accord with the remark made in Sec. I about the applicability of the Yukawa potential in 2D dusty plasmas [5,6], we have neglected here the ion flow perpendicular to the dust layer immersed in a plasma sheath, expecting that the related downstream ion wake will have little effect on the fluid dynamics within the layer. Such an approximation may not work too well for describing any flexural wave modes accompanied by particle oscillations in the direction perpendicular to the layer.

The above equations can be solved perturbatively [19,25], giving a dielectric function of the 2D dust fluid in the form

$$\varepsilon(k,\omega) = 1 - \frac{2\pi e^2 Z_d^2 \sigma_{d0}}{m\lambda_D} \frac{k^2\lambda_D^2}{\sqrt{k^2\lambda_D^2+1}} \frac{1}{\omega(\omega+i\nu)}. \tag{8}$$

We define

$$\omega_0^2(k) = \frac{2\pi e^2 Z_d^2 \sigma_{d0}}{m\lambda_D} \frac{(\lambda_D k)^2}{\sqrt{k^2\lambda_D^2+1}} \equiv \frac{\sigma_{d0}}{m}\tilde{\phi}(k)k^2, \tag{9}$$

and note that $\tilde{\phi}(k)$ is the 2D Fourier transform of the Yukawa potential, as expected. A dispersion relation for acoustic waves in the 2D dust fluid [25] can be obtained from

$$\omega(\omega+i\nu) = \omega_0^2(k), \tag{10}$$

in analogy to the 3D case [1,2,22,23]. The real part of the dispersion is shown in Fig. 2 (heavy dashed lines), while the corresponding discussion is postponed to Sec. III B.

B. DTW

Note that in the above derivation, we have assumed that the dust fluid is cold and, consequently, we neglected the direct thermal effect. Nevertheless, it would be interesting to see how this effect changes the wave dispersion in the dust fluid. This effect can be easily retained by including the ideal-gas part of pressure, P_{dk}, in the momentum balance equation, Eq. (6), as follows [23]:

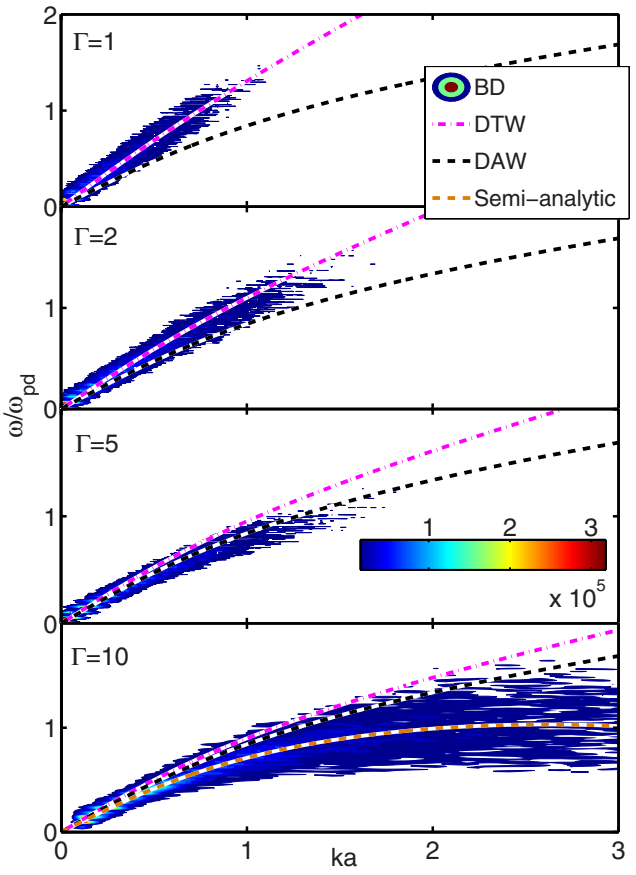

FIG. 2. (Color online) (Color bar in arbitrary units) Wave spectra of the longitudinal mode for $\kappa=1$, $\nu=0.01\omega_{pd}$, and different Γ values covering nonideal gas states. The black and white dashed lines are the dispersion relations of the DAW, while the pink (gray) dash-dotted lines are the results of the DTW. The semianalytic approximation is shown by the brown (light gray and white) lower dashed line in the panel for $\Gamma=10$.

$$\frac{\partial \mathbf{u}_d(\mathbf{r},t)}{\partial t} + \mathbf{u}_d(\mathbf{r},t)\cdot\nabla_\parallel \mathbf{u}_d(\mathbf{r},t) = \frac{eZ_d}{m}\nabla_\parallel \Phi(\mathbf{R},t)|_{z=0} - \nu\mathbf{u}_d(\mathbf{r},t) + \frac{1}{m\sigma_{d0}}\nabla_\parallel P_{dk}, \tag{11}$$

where $P_{dk} = \gamma_d k_B T \sigma_d$ is the kinetic part of pressure in the dust component, and $\gamma_d = 2$ is the adiabatic index for the 2D dust system [23].

With this new momentum balance equation, the dielectric function of the 2D dust fluid becomes

$$\varepsilon(k,\omega) = 1 - \frac{1}{\omega(\omega+i\nu)}\left[\omega_0^2(k) + \frac{\gamma_d v_{\text{th}}^2}{2}k^2\right], \tag{12}$$

with $v_{\text{th}} = \sqrt{2k_BT/m}$ being the thermal speed of dust particles, which gives the dispersion relation for DTW as

$$\omega(\omega+i\nu) = \omega_0^2(k) + \frac{\gamma_d v_{\text{th}}^2}{2}k^2. \tag{13}$$

The real part of the DTW dispersion is shown in Fig. 2 (dash-dotted lines).

One expects that the DAW and DTW modes, derived above, should be dominant in weakly coupled systems. However, to the best of our knowledge, this conjecture has not been examined in previous simulations. To elucidate this issue, we show in Fig. 2 the wave spectra from our simulations, together with the dispersion relations for both the DAW and DTW for very low coupling strengths, at which systems are often regarded as being in a nonideal gaseous state. One sees that, at such high temperatures, the collective modes are heavily damped at short wavelengths. There are essentially no collective modes beyond $ka=2$ for $\Gamma=1$, 2, and 5 and, moreover, these modes decrease in amplitude at higher temperatures, or lower Γs. One would attribute this to Landau damping and/or viscous/collisional damping. Comparison with the above analytical results at $\Gamma=1$ shows that the agreement between the DTW and the simulation is remarkably good, whereas the DAW displays noticeable discrepancy with simulation, indicating that the thermal effect is significant. With increasing Γ or, equivalently, decreasing temperature, a discrepancy between the DTW and simulation develops and becomes noticeable at, e.g., $\Gamma=5$, whereas the DAW seems to agree better with simulation. However, this seemingly improved agreement between the DAW and simulation at $\Gamma=5$ is just a coincidence because the direct thermal effect and the strong-coupling effect tend to cancel each other, as will be shown in Sec. III C. In fact, a discrepancy arises immediately when Γ increases further, say, above $\Gamma=10$.

C. Semianalytic approximation

The DAW and DTW derived in Secs. III A and III B are essentially based on the continuum mean-field theory of the RPA type [22,23], in which discreteness of particles is neglected. Therefore, the above results are applicable, in principle, only in the weakly coupled situations, i.e., when $\Gamma \ll 1$. For strongly coupled systems, short-range interparticle interactions become important, and it is necessary to take this local-field effect into account. This can be achieved in an approximate manner, even within the fluid model, by introducing a correction, P_{di}, to the ideal-gas pressure term in the momentum balance equation, as follows [25,47]:

$$\frac{\partial \mathbf{u}_d(\mathbf{r},t)}{\partial t} + \mathbf{u}_d(\mathbf{r},t)\cdot\nabla_\parallel \mathbf{u}_d(\mathbf{r},t) = \frac{eZ_d}{m}\nabla_\parallel \Phi(\mathbf{R},t)|_{z=0} - \nu \mathbf{u}_d(\mathbf{r},t) + \frac{1}{m\sigma_{d0}}\nabla_\parallel P_{dk} + \frac{1}{m\sigma_{d0}}\nabla_\parallel P_{di}, \tag{14}$$

where P_{di} contains information on the system structure and short-range interactions. Progress toward semianalytic results for dielectric function [15,25] can be made by writing

$$\nabla_\parallel P_{di} = \left(\frac{\delta P_{di}}{\delta \sigma_d}\right)_T \nabla_\parallel \sigma_d, \tag{15}$$

where $\alpha \equiv (\delta P_{di}/\delta\sigma_d)_T$ is recognized as the isothermal dust layer compressibility [29,47], which can be further expressed using the density-functional theory as [25]

$$\alpha = \frac{\sigma_{d0}}{m}\frac{\partial^2}{\partial \sigma_{d0}^2}[\sigma_{d0}\epsilon_c(\sigma_{d0})], \tag{16}$$

with ϵ_c being the system's correlation energy. (See Ref. [25] and references therein for details of the derivation.) We note that an empirical expression for ϵ_c for a 2D Yukawa system is now available through computer simulation [48]. One finally obtains [15,25]

$$\varepsilon(k,\omega) = 1 - \frac{1}{\omega(\omega+i\nu)-\alpha k^2}\left[\omega_0^2(k) + \frac{\gamma_d v_{\rm th}^2}{2}k^2\right], \tag{17}$$

giving the dispersion relation in the form

$$\omega(\omega+i\nu) = \omega_0^2(k) + \frac{\gamma_d v_{th}^2}{2}k^2 + \alpha k^2. \tag{18}$$

We remark that the term with α in Eq. (17) can be regarded as primitive form of a local-field correction (LFC) to the mean-field theory, which accounts for the strong-coupling effects [47]. Because α is related to the correlation energy ϵ_c, which in turn can be obtained from simulations [48], we adopt the term semianalytic approximation for the above dispersion relation, coined by Dubin [15]. Typical values of α are about $-0.25(\omega_{pd}a)^2$.

It should be noted that in Eq. (18) the direct thermal effect and the correlation effect exert opposite influences on the dispersion relation. At very high temperatures, say $\Gamma=1$, the correlation effect is negligibly small so we see in Fig. 2 perfect agreement between the DTW dispersion and the simulation. With increasing Γ, the direct thermal effect decreases in magnitude while the correlation effect becomes more pronounced. Since $\alpha \propto -\Gamma v_{th}^2$ [49], the two effects should cancel each other for some value of Γ. We see a good agreement between the DAW dispersion and the simulation in Fig. 2 at around $\Gamma=5$. As can be expected, with further increase in Γ, the correlation effect becomes dominant so that the semianalytic dispersion shows best agreement with simulation at $\Gamma=10$, as shown in Fig. 2. We note that similar effect was also observed in the GH theory of Kaw and Sen [29] for 3D dusty plasma liquids.

D. QLCA

In Sec. III C, we have introduced a primitive LFC via density functionals for the interaction part of the dust pressure. A more appropriate way of introducing the LFC into the RPA theory was achieved in terms of the QLCA [18,26,35], which was found quite successful in describing the collective dynamics in SCDPs [18,19,35]. The corresponding dielectric function (for both the longitudinal and transverse modes) of a 2D SCDP can be written as

$$\varepsilon_{L/T}(k,\omega) = 1 - \frac{\omega_0^2(k)}{\omega(\omega+i\nu)-D_{L/T}(k)}, \tag{19}$$

where $D_L(k)$ and $D_T(k)$ are projections of the dynamical matrix in the longitudinal and transverse directions, respectively. We note that $D_L(k)$ and $D_T(k)$ are functionals of the equilibrium radial distribution function, $g(r)$, and their detailed expressions can be found in Refs. [18,35,39]. It is im-

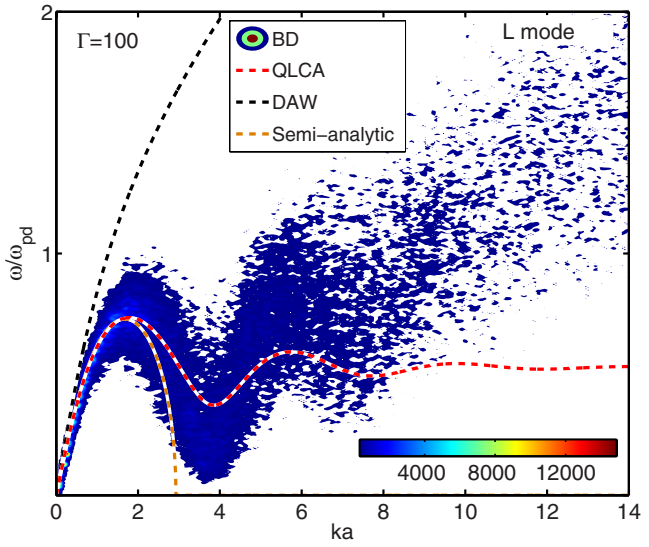

FIG. 3. (Color online) (Color bar in arbitrary units) Wave spectra of the longitudinal mode for $\kappa=1$, $\Gamma=100$, and $\nu=0.01\omega_{pd}$. The black dashed upper curve shows the dispersion relation of the DAW, the red (gray and white) dashed middle curve shows the QLCA, and the brown (light gray and white) dashed lower curve shows the semianalytic approximation.

portant to remark here that the direct thermal effect is neglected in standard formulations of the QLCA, but we shall discuss approximate ways of how to include this effect in Sec. IV.

The longitudinal and transverse modes are determined from the above dielectric functions by letting

$$\varepsilon_L(k,\omega)=0, \quad \text{and} \quad \varepsilon_T^{-1}(k,\omega)=0, \tag{20}$$

which give the respective dispersion relations as

$$\omega(\omega+i\nu)=\omega_0^2(k)+D_L(k), \tag{21}$$

$$\omega(\omega+i\nu)=D_T(k). \tag{22}$$

Figure 3 shows a longitudinal phonon spectrum for $\Gamma=100$ and $\nu=0.01\omega_{pd}$. Also shown are dispersion relations of the DAW, the semianalytic approximation, and the QLCA. A good agreement between the simulation and the QLCA is clearly seen in a broad range of wavelengths on the long-wavelength side, as expected [18,19,35]. Discrepancy appears beyond the first Brillouin zone, especially for very large wave numbers, where the simulation displays a raising tail due to the DTW mode, while the QLCA dispersion converges to the Einstein frequency [18,26]. This discrepancy is a consequence of the neglect of the direct thermal effects in the QLCA, which prompts us to discuss a suitable amendment to this theory, to be described in Sec. III E. It is not surprising to find that the result of the semianalytic approximation essentially coincides with the QLCA in the long-wavelength region (up to around $ka=2.0$), because actually $\alpha=\lim_{k\to 0} D_L(k)/k^2$ [18,26,35]. However, the semianalytic approximation breaks down for short wavelengths because local-field effects arise from the length scales $\sim a$ that cannot be treated properly within the fluid model.

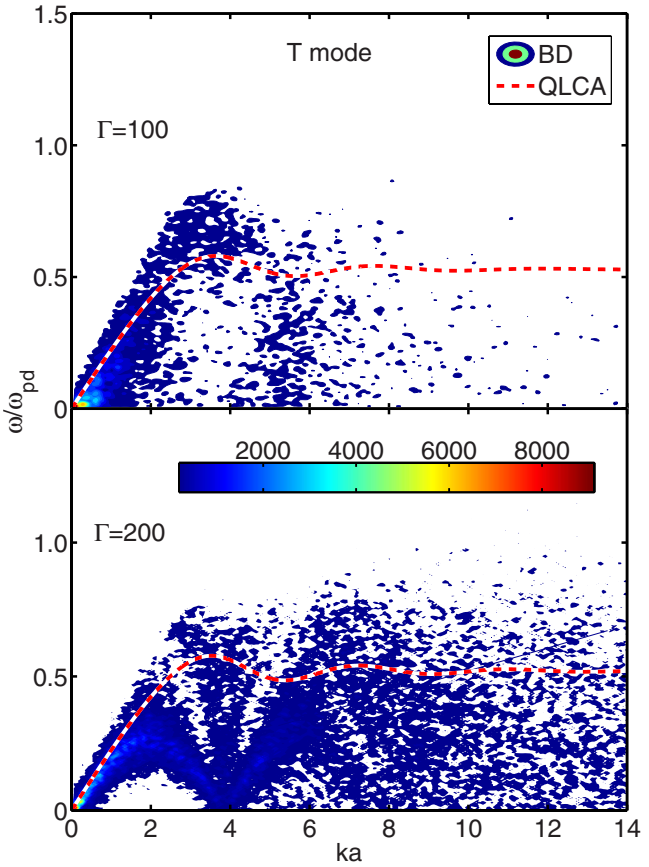

FIG. 4. (Color online) (Color bar in arbitrary units) Wave spectra of the transverse mode for $\Gamma=100$ and 200, $\kappa=1$, and $\nu=0.01\omega_{pd}$. The red (gray and white) dashed lines show the dispersion relation of the QLCA.

Figure 4 shows the wave spectra of a transverse mode with $\nu=0.01\omega_{pd}$, for $\Gamma=100$ and 200, along with a dispersion relation from the QLCA. The transverse mode is heavily damped, especially at short wavelengths and in the system at a higher temperature (lower Γ), as can be seen from Fig. 4. For $\Gamma=100$, there are practically no transverse modes beyond $ka\approx 6$ (implying a short-wavelength cutoff) while, for $\Gamma=200$, the spectrum becomes very noisy beyond $ka\approx 6$ so that it is difficult to distinguish peaks due to collective motion. One can also notice that, for $\Gamma=100$, the peak contour of the wave spectra does not seem to approach $ka=0$ at $\omega=0$, indicating that there exists a long-wavelength cutoff [31]. (This feature will be further discussed below.) Agreement between the simulation and the QLCA does not appear to be very satisfactory, neither at short nor at long wavelengths. The agreement at long wavelengths is somewhat improved for $\Gamma=200$, in which case the long-wavelength cutoff vanishes. It should be noted that the melting point for this system occurs at $\Gamma^*\approx 180$ for $\kappa=1$ [18]. So at $\Gamma=200$, particles are almost frozen and the wave propagation at short wavelengths becomes anisotropic. The task of resolving angular dependence of the wave dispersion lies beyond the capability of the QLCA, but this issue can be tackled with the HA, as shown below.

E. QLCA with DTW in longitudinal mode

It is known [18,26,35] that the QLCA neglects the direct thermal effect which is responsible for the Brownian motions and migrations of individual dust particles. This effect also gives rise to the so-called Bohm-Gross term ($\propto k^2 v_{th}^2$) in the third-frequency-momentum sum rule and, consequently, in the longitudinal dispersion relation [26]. Since this term is of the order of $\sim\Gamma^{-1}$ in comparison with terms due to the correlation effect, it is a good approximation to neglect it for $\Gamma \gg 1$ and, especially, at long wavelengths, $ka \ll 1$. However, at short wavelengths, $ka \gg 1$, the k^2 factor could elevate the direct thermal effect up to a significant level. Nevertheless, this effect was not examined in previous simulations and is, therefore, of interest for the present study.

A simple extension of the QLCA, which would include the effect of direct thermal motion, can be made at the phenomenological level by taking into account a contribution from the kinetic part of pressure, as defined in the subsection on DTW. Mathematically, this can be done by inserting the QLCA-LFC function $D_L(k)$ into the denominator of Eq. (12), or by replacing the term αk^2 in Eq. (17) with $D_L(k)$. This gives an approximately extended QLCA dielectric function for the longitudinal mode as

$$\varepsilon(k,\omega) = 1 - \frac{1}{\omega(\omega + i\nu) - D_L(k)}\left[\omega_0^2(k) + \frac{\gamma_d v_{th}^2}{2}k^2\right], \tag{23}$$

and the corresponding longitudinal dispersion relation as

$$\omega(\omega + i\nu) = \omega_0^2(k) + D_L(k) + \frac{\gamma_d v_{th}^2}{2}k^2. \tag{24}$$

Figure 5 shows the wave spectra of the longitudinal mode for different values of Γ covering a wide range in both the liquid and solid states. Dispersion relations of both the DAW and the QLCA with the above DTW extension (denoted as EQLCA), Eq. (24), are also shown for comparison. It is seen that the EQLCA exhibits a consistently good agreement with the simulation at small wave numbers, while capturing the raising DTW tails at large wave numbers. Those DTW tails in the displayed spectra become less and less significant with increasing Γ, but the DTW mode is still noticeable, even at $\Gamma=800$, although it is very weak there. On the other hand, discrepancies still exist in some fine structures, seen in Fig. 5 at intermediate wave numbers. Some of those discrepancies, occurring for $\Gamma > \Gamma^*$, are due to the angular dependence of wave propagation in the solid state.

It should be noted here that the above extension is essentially based on the mean-field theory of Rao [23], and that the QLCA is used only to provide an LFC factor. Therefore, from this point of view, our extension is not strictly self-consistent and might not satisfy the third-frequency sum rule. A more self-consistent theory, which can satisfy the third-frequency sum rule, is now under development and will be presented elsewhere [50].

F. QLCA with critical wave cutoff in transverse mode

An another weakness of the QLCA lies in its inability to account for the diffusional and other damping effects that

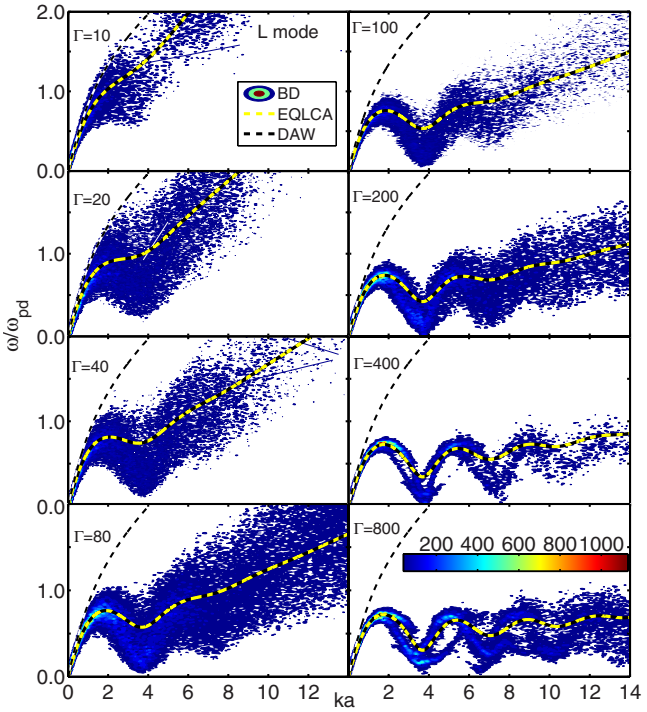

FIG. 5. (Color online) (Color bar in arbitrary units) Wave spectra of the longitudinal mode for $\kappa=1$, $\nu=0.01\omega_{pd}$, and different Γ values covering both the liquid and solid states. The thin black dashed upper lines are the results of the DAW, while the thick yellow (light gray) lower dashed lines show the extension of the QLCA with the DTW mode, labeled EQLCA

preclude the existence of the long-wavelength transverse waves in the liquid state [18,35]. Kalman *et al.* [18] provided a work-around by introducing a phenomenological damping ν_{DM}. This gives rise to a small change in the transverse dielectric function in the QLCA,

$$\varepsilon(k,\omega) = 1 - \frac{\omega_0^2(k)}{\omega(\omega + i\nu + i\nu_{DM}) - D_T(k)}, \tag{25}$$

and consequently in the transverse dispersion relation,

$$\omega(\omega + i\nu + i\nu_{DM}) = D_T(k). \tag{26}$$

By assuming $\nu=0^+$, the real part of the dispersion relation can be written as

$$\omega_r = \sqrt{D_T(k) - \frac{\nu_{DM}^2}{4}}, \tag{27}$$

so that the condition $D_T(k) - \nu_{DM}^2/(4) \geq 0$ gives rise to a critical cutoff wave number k_c.

Note that ν_{DM}, and consequently k_c, can be determined by directly fitting the simulation results to the above form [18]. Results of such fitting are shown in Fig. 6, along with a magnification of Fig. 4 at small wave numbers k, where one can clearly notice the existence of a long-wavelength cutoff k_c. As a consequence of the above extension to the transverse dielectric function in the QLCA, one can see an improved agreement between the simulation and the dispersion relation, Eq. (27). This extension of the QLCA does not affect

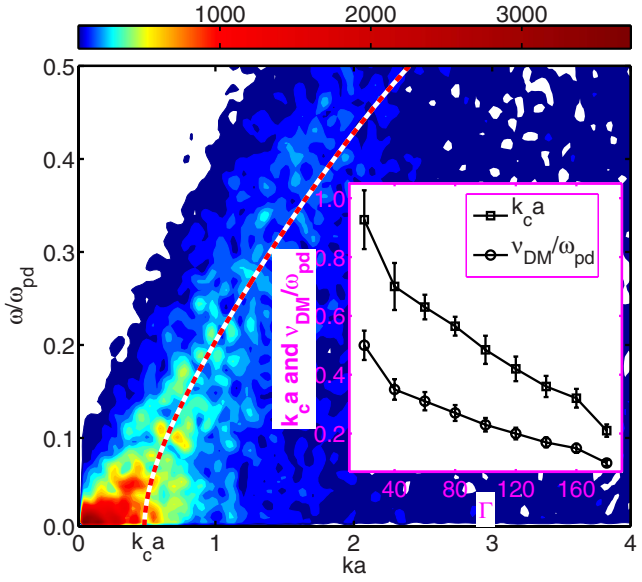

FIG. 6. (Color online) (Color bar in arbitrary units) Wave spectra of the transverse mode for $\Gamma=100$, $\kappa=1$, and $\nu=0.01\omega_{pd}$. The red (gray and white) dashed line is the fit according to Eq. (27), i.e., the extension of the QLCA with a cutoff wave number k_c. The fit gives $\nu_{DM}\approx 0.23\omega_{pd}$ and $k_c a=0.48$. The inserted figure shows the fitted values of $k_c a$ and ν_{DM}/ω_{pd} as functions of Γ for $\kappa=1$ and $\nu=0.01\omega_{pd}$.

much the dispersion at large k, where it behaves in much the same way as in Fig. 4, because $\nu_{DM}\approx 0.23\omega_{pd}$ is relatively small. From the figure's inset, one sees that the cutoff wave number k_c increases with decreasing Γ. This tendency agrees with previous experimental observations [12].

G. HA for DLW

In a perfect crystalline state, all particles are located at the points of a triangular lattice, and they perform thermal oscillations around their equilibrium positions. In this case, one needs to adopt an another strategy to obtain dispersion relation for the DLW. This dispersion relation can be determined from the following eigenvalue problem [15]:

$$\|\omega^2(\mathbf{k})\mathbf{I}-\mathbf{M}(\mathbf{k})\|=0, \tag{28}$$

where $\mathbf{I}$ is the 2D unit matrix. [Note that, although we have neglected the phenomenological damping in Eq. (28), it can be easily retained by replacing ω^2 with $\omega(\omega+i\nu)$.] The matrix $\mathbf{M}(\mathbf{k})$ is the interaction matrix, given by [15]

$$\mathbf{M}(\mathbf{k})=\frac{1}{m}\sum_i \frac{\partial^2\phi}{\partial\mathbf{r}_i\,\partial\mathbf{r}_i}[1-e^{i\mathbf{k}\cdot\mathbf{r}_i}]\equiv[M_{\alpha\beta}(\mathbf{k})], \tag{29}$$

where α and $\beta=x,y$, and the summation over i includes all points on the triangular lattice.

The results for dispersion in the HA [15] are quite similar to those of the QLCA. There are two branches, given by

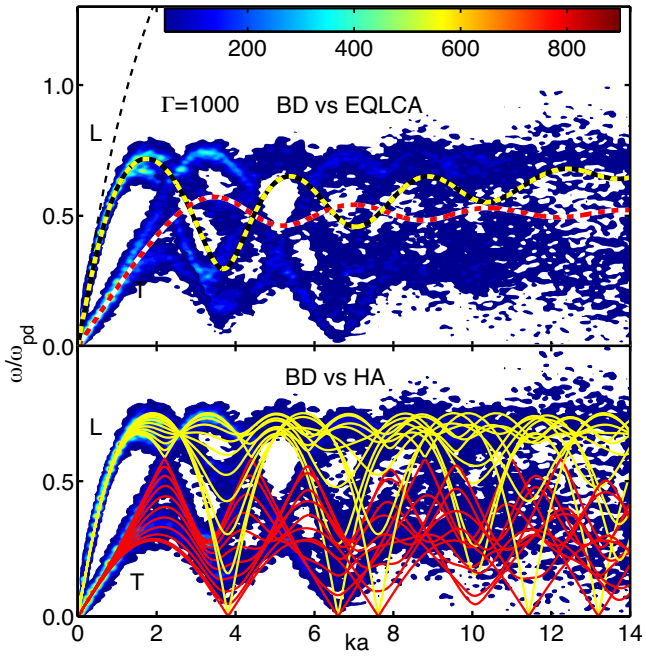

FIG. 7. (Color online) (Color bar in arbitrary units) Wave spectra of both the longitudinal (L) and transverse (T) modes for $\kappa=1$, $\Gamma=1000$, and $\nu=0.01\omega_{pd}$. In the upper panel, the upper yellow (light gray) dashed curve shows the L mode and the lower red (gray and white) dashed curve shows the T mode of the EQLCA dispersions, while the black dashed curve shows the DAW dispersion. In the lower panel, the upper set of yellow (light gray) continuous curves show the L modes and the lower set of red (gray) continuous curves show the T modes of the HA dispersions, with both sets covering the period $\pi/6$ of the propagation directions with an increment of 3 degrees.

$$\omega^2_{L/T}(k,\theta)=\tfrac{1}{2}[M_{xx}+M_{yy}] \pm \tfrac{1}{2}\sqrt{[M_{xx}+M_{yy}]^2+4(M^2_{xy}-M_{xx}M_{yy})}, \tag{30}$$

where $M_{\alpha\beta}$ is given by Eq. (29) and θ is the polarization angle [15]. The subscripts L and T denote the longitudinal and transverse modes, and they correspond to the signs + and − in Eq. (30), respectively. Therefore, wave propagation depends on the angle θ, and the dispersion relations are functions with the period of $\pi/6$ due to the hexagonal symmetry [15]. The angular dependence arises because the system is now anisotropic at short wavelengths.

Figure 7 shows the wave spectra of both the longitudinal and transverse modes in a crystalline state with $\Gamma=1000$. Also shown are the dispersion relations of the HA, EQLCA, and DAW. The HA curves cover the whole period of $\pi/6$, shown with an increment of 3 degrees. It is seen that the simulation agrees very well with the HA, and that the polarization effects in the simulation spectra are fully captured by the HA. Good agreement between the EQLCA and the simulation is retained in the first Brillouin zone. For large wave numbers, the EQLCA cannot resolve the polarization, i.e., the angular dependence of the dispersion. Nevertheless, it captures the correct tendency for oscillations. Moreover, at

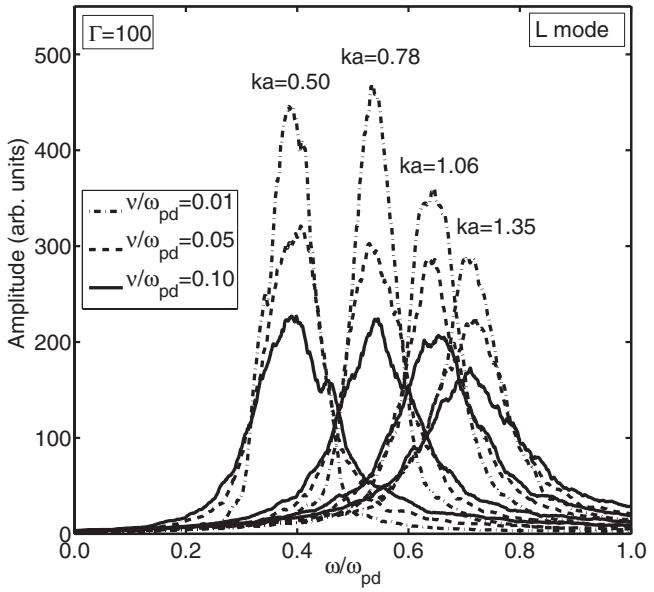

FIG. 8. Profiles of the longitudinal wave spectra (in arbitrary units) for several values of the wave number k, with $\kappa=1$, $\Gamma=100$, and for several damping rates on the neutral gas ν.

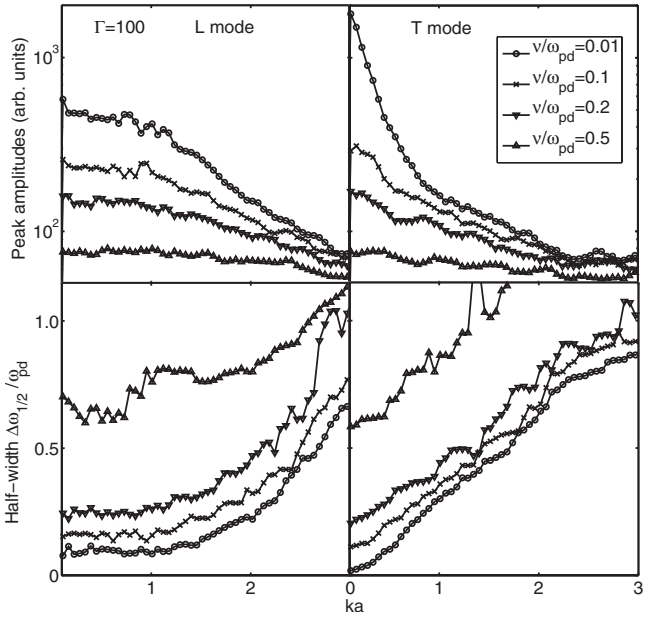

FIG. 9. The peak amplitudes (upper panels, in arbitrary units) and the half-widths $\Delta\omega_{1/2}$ (lower panels, in units of ω_{pd}) of both the longitudinal (left panels) and transverse (right panels) wave spectra, shown as functions of the reduced wave number ka for $\kappa=1$, $\Gamma=100$, and for several damping rates on the neutral gas ν.

this range of Γ values, the QLCA regains its credibility because both the thermal effect and the long-wavelength cutoff corrections become unimportant, and the EQLCA essentially reduces to the standard QLCA. At the same time, it is remarkable to see that the mean-field DAW is so robust, even in a crystalline state, where it still offers a fairly good agreement with the simulation at long wavelengths.

H. Damping effect

We finally investigate the effects of damping on wave spectra. Generally speaking, there are two types of damping mechanisms for collective modes, i.e., the intrinsic and the external ones. The former type includes damping due to diffusion, viscosity, thermal conduction, and, possibly, also Landau-like damping [26,46,47], while the latter type mainly comes from the neutral gas. The external damping is simply given by the imaginary part of the dispersion relation as $\omega_i=-\nu/2$, whereas the intrinsic damping of collective modes involves complicated physical processes and, so far, there has been no well founded theory of such processes for SCDPs. While development of such a theory may be an interesting topic for future research, at this stage, we just present and discuss several results from our simulation.

Figure 8 shows the profiles, or, more precisely the cross sections at several fixed wave numbers, of the longitudinal wave spectra, $\mathcal{L}(\mathbf{k},\omega)$, for $\Gamma=100$ and with different neutral-gas damping rates ν. These profiles exhibit typical resonance shapes which describe the spectral distributions shown in Figs. 1–7, while their peak positions in the ω-k plane correspond to the dispersion relations obtained from the above-mentioned analytical theories. In reality, these peaks are never deltalike functions, but rather have finite amplitudes and finite widths due to various damping effects, as is shown in Fig. 8. Physically, the peak amplitudes indicate the amount of energy concentrated in various collective modes, while the widths of the peaks at half heights (denoted as the half-widths, $\Delta\omega_{1/2}$) are related to various mechanisms of the energy dissipation out of those modes [9]. One notices a general tendency that the peak amplitudes decrease, while the corresponding widths increase with increasing wave numbers. In addition, with the increase in the neutral-gas damping rate ν, all amplitudes decrease and the widths increase, as expected. Those trends are depicted more clearly in Fig. 9, which shows the amplitudes and the half-widths of $\mathcal{L}(\mathbf{k},\omega)$ and $\mathcal{T}(\mathbf{k},\omega)$ versus the wave number for different ν.

The observed decrease in amplitudes and increase in widths with increasing wave numbers deserve special attention. A simple explanation comes from the fact that when the wavelengths become shorter than about the average interparticle separation, the energy concentrated in collective modes is dissipated mainly into the single-particle excitations, which are typically described by broad features in the measured spectra. These excitations are expected to further give rise to the heating of dusty plasmas, where the system temperature plays an important role, as was found for the direct thermal effect in the wave spectra shown in Fig. 5 at short wavelengths.

Furthermore, the dependencies of the widths $\Delta\omega_{1/2}$ on the wave number k, shown in Fig. 9, are particularly intriguing. Asserting that a collective mode is well defined if the associated width is (much) smaller than the corresponding peak frequency, i.e., the dispersion relation $\omega(k)$, one can explain why the wave spectra of the transverse mode shown in Fig. 4 appear more "noisy," even at long wavelengths, than the corresponding spectra of the longitudinal mode, shown in Figs. 3 and 5. Namely, that observation can be traced back to the Fig. 9, showing an almost linear increase in the width $\Delta\omega_{1/2}$

with ka for the transverse mode, as opposed to a power-law-like increase for the longitudinal mode of the form $\Delta\omega_{1/2} \sim (ka)^p$ with $p>1$, at small values of ka.

IV. CONCLUSION

By using the Brownian dynamics simulation, we have investigated the wave spectra of 2D dusty plasmas in the states that cover full range from a nonideal gas to a crystalline state. These results are critically compared with dispersion relations resulting from various theoretical models, such as the dust-acoustic wave, dust-thermal wave, quasilocalized charge approximation, and the harmonic approximation. In particular, simple extensions are considered that introduce the direct thermal effect and the critical cutoff wave number into the QLCA. It is found that, for a nonideal gaseous state (e.g., with $\Gamma=1$), the longitudinal DTW is in a remarkably good agreement with the simulation, while for a perfect crystalline state (e.g., $\Gamma=1000$), the HA agrees very well with the simulation. In the states with Γ between those two opposing limits, an overall good agreement between the extended versions of the QLCA and the simulation was found for a wide range of wavelengths, whereas a semianalytic approximation for the local-field correction to the DTW dispersion relation works well at long wavelengths, say $ka<2$.

The damping effect is also briefly discussed in terms of the peak amplitudes and the half-widths of the current-current correlation functions for different neutral-gas damping rates ν and different wavelengths. A general trend was found that the peak amplitudes decrease and the widths increase with increasing wave numbers and increasing ν. In view of our critical analysis of various analytical theories for dispersion relations in dusty plasmas, a conceptual question arises as to under what conditions one may even speak of a well-defined collective mode with the dispersion frequency $\omega(k)$. If one adopts a criterion that the corresponding half-width $\Delta\omega_{1/2}(k)$ needs to be sufficiently smaller than the frequency of the mode $\omega(k)$, our results indicate that, e.g., longitudinal modes at intermediate Γs are well defined at sufficiently long wavelengths only, say $ka<2$, even with the smallest damping rates ν used in the present simulation. Future computational studies of the wave spectra will be used to reveal further details on structure and dynamics of SCDPs.

ACKNOWLEDGMENTS

L.J.H. acknowledges support from Alexander von Humboldt Foundation. Work at CAU is supported by DFG within Grant No. SFB-TR24/A2. Z.L.M. acknowledges support from NSERC. L.J.H. thanks Professor Z. Donkó and Professor P. K. Shukla for valuable discussions.

[1] P. K. Shukla, Phys. Plasmas **8**, 1791 (2001).
[2] P. K. Shukla and A. A. Mamun, *Introduction to Dusty Plasma Physics* (Institute of Physics, Bristol, 2002).
[3] P. K. Shukla and B. Eliasson, Rev. Mod. Phys. **81**, 25 (2009).
[4] M. Lampe, G. Joyce, and G. Ganguli, Phys. Plasmas **7**, 3851 (2000); IEEE Trans. Plasma Sci. **33**, 57 (2005).
[5] U. Konopka, G. E. Morfill, and L. Ratke, Phys. Rev. Lett. **84**, 891 (2000).
[6] D. S. Lemons, M. S. Murillo, W. Daughton, and D. Winske, Phys. Plasmas **7**, 2306 (2000).
[7] A. Homann, A. Melzer, S. Peters, and A. Piel, Phys. Rev. E **56**, 7138 (1997).
[8] A. Homann, A. Melzer, S. Peters *et al.*, Phys. Lett. A **242**, 173 (1998).
[9] S. Nunomura, J. Goree, S. Hu, X. Wang, A. Bhattacharjee, and K. Avinash, Phys. Rev. Lett. **89**, 035001 (2002).
[10] S. Zhdanov, S. Nunomura, D. Samsonov, and G. Morfill, Phys. Rev. E **68**, 035401(R) (2003).
[11] S. Nunomura, S. Zhdanov, D. Samsonov, and G. Morfill, Phys. Rev. Lett. **94**, 045001 (2005).
[12] V. Nosenko, J. Goree, and A. Piel, Phys. Rev. Lett. **97**, 115001 (2006).
[13] F. M. Peeters and X. Wu, Phys. Rev. A **35**, 3109 (1987).
[14] F. Melandsø, Phys. Plasmas **3**, 3890 (1996).
[15] D. H. E. Dubin, Phys. Plasmas **7**, 3895 (2000).
[16] X. Wang, A. Bhattacharjee, and S. Hu, Phys. Rev. Lett. **86**, 2569 (2001).
[17] M. S. Murillo and D. O. Gericke, J. Phys. A **36**, 6273 (2003).
[18] G. J. Kalman, P. Hartmann, Z. Donko, and M. Rosenberg, Phys. Rev. Lett. **92**, 065001 (2004).
[19] A. Piel and J. Goree, Phys. Plasmas **13**, 104510 (2006).
[20] T. Sullivan, G. J. Kalman, S. Kyrkos, P. Bakshi, M. Rosenberg, and Z. Donkó, J. Phys. A **39**, 4607 (2006).
[21] P. Hartmann, Z. Donkó, G. J. Kalman, S. Kyrkos, M. Rosenberg, and P. Bakshi, IEEE Trans. Plasma Sci. **35**, 337 (2007).
[22] N. N. Rao, P. K. Shukla, and M. Y. Yu, Planet. Space Sci. **38**, 543 (1990).
[23] N. N. Rao, Phys. Plasmas **7**, 795 (2000).
[24] L. Stenflo, P. K. Shukla, and M. Y. Yu, Phys. Plasmas **7**, 2731 (2000); L. Stenflo and P. K. Shukla, *ibid.* **7**, 3472 (2000).
[25] L. J. Hou, Y. N. Wang, and Z. L. Mišković, Phys. Rev. E **70**, 056406 (2004).
[26] K. I. Golden and G. J. Kalman, Phys. Plasmas **7**, 14 (2000).
[27] M. Rosenberg and G. Kalman, Phys. Rev. E **56**, 7166 (1997).
[28] G. Kalman, M. Rosenberg, and H. E. DeWitt, Phys. Rev. Lett. **84**, 6030 (2000).
[29] P. K. Kaw and A. Sen, Phys. Plasmas **5**, 3552 (1998).
[30] M. S. Murillo, Phys. Plasmas **5**, 3116 (1998).
[31] M. S. Murillo, Phys. Rev. Lett. **85**, 2514 (2000).
[32] M. S. Murillo, Phys. Plasmas **7**, 33 (2000).
[33] D. Winske, M. S. Murillo, and M. Rosenberg, Phys. Rev. E **59**, 2263 (1999).
[34] H. Ohta and S. Hamaguchi, Phys. Rev. Lett. **84**, 6026 (2000).
[35] Z. Donkó, G. J. Kalman, and P. Hartmann, J. Phys.: Condens. Matter **20**, 413101 (2008).
[36] M. P. Allen and D. J. Tildesley, *Computer Simulation of Liquids* (Oxford University Press, New York, 1989).
[37] L. J. Hou and Z. L. Mišković, e-print arXiv:0806.3912.

[38] L. J. Hou, and Z. L. Mišković, A. Piel and P. K. Shukla, e-print arXiv:0904.2849.
[39] K. Jiang, L. J. Hou, Y. N. Wang, and Z. L. Mišković, Phys. Rev. E **73**, 016404 (2006).
[40] L. J. Hou, Z. L. Mišković, K. Jiang, and Y. N. Wang, Phys. Rev. Lett. **96**, 255005 (2006).
[41] L. J. Hou and Z. L. Mišković, Phys. Rev. E **77**, 046401 (2008).
[42] L. J. Hou and A. Piel, Phys. Plasmas **15**, 073707 (2008).
[43] L. J. Hou and A. Piel, J. Phys. A: Math. Theor. (to be published); e-print arXiv:0810.1623.
[44] L. J. Hou, A. Piel, and P. K. Shukla, Phys. Rev. Lett. **102**, 085002 (2009).
[45] V. E. Fortov, O. S. Vaulina, O. F. Petrov *et al.*, Phys. Rev. Lett. **90**, 245005 (2003).
[46] J. P. Boon and S. Yip, *Molecular Hydrodynamics* (Dover, New York, 1991).
[47] S. Ichimaru, *Statistical Plasma Physics II: Condensed Plasmas* (Westview, Boulder, 2004), Chap. 3.
[48] P. Hartmann, G. J. Kalman, Z. Donkó, and K. Kutasi, Phys. Rev. E **72**, 026409 (2005).
[49] This was pointed out by one of the referees.
[50] M. S. Murillo (unpublished).